

Pulsar recoil by large-scale anisotropies in supernova explosions

L. Scheck,¹ T. Plewa,^{2,3} H.-Th. Janka,¹ K. Kifonidis,¹ and E. Müller¹

¹*Max-Planck-Institut für Astrophysik, Karl-Schwarzschild-Str. 1, D-85741 Garching, Germany*

²*Center for Astrophysical Thermonuclear Flashes,*

University of Chicago, 5640 S. Ellis Avenue, Chicago, IL 60637, USA

³*Nicolaus Copernicus Astronomical Center, Bartycka 18, 00716 Warsaw, Poland*

(Dated: December 6, 2018)

Assuming that the neutrino luminosity from the neutron star core is sufficiently high to drive supernova explosions by the neutrino-heating mechanism, we show that low-mode ($l = 1, 2$) convection can develop from random seed perturbations behind the shock. A slow onset of the explosion is crucial, requiring the core luminosity to vary slowly with time, in contrast to the burst-like exponential decay assumed in previous work. Gravitational and hydrodynamic forces by the globally asymmetric supernova ejecta were found to accelerate the remnant neutron star on a timescale of more than a second to velocities above 500 km s^{-1} , in agreement with observed pulsar proper motions.

PACS numbers: 97.60.Bw, 97.60.Gb, 95.30.Jx, 95.30.Lz

Young pulsars are observed to have average space velocities of $200\text{--}500 \text{ km s}^{-1}$ with highest values above 1000 km s^{-1} and still ambiguous hints for a double peak distribution [1]. There is no clear statistical correlation with the magnetic moment or rotation of the pulsar, although in two cases (Vela and Crab) the direction of motion appears to be aligned with the spin axis.

A connection of the pulsar motions with the supernova (SN) explosion is suggested by neutron star (NS)–SN remnant associations and by the properties of binary systems with one or both components being a NS. Natal kicks are required, e.g., by the spin-orbit misalignment and high orbital eccentricities observed in some binaries (for a review, see [2]).

Various mechanisms have been proposed to explain these kicks. One possibility invokes asymmetric mass ejection during the SN [3]. This may be caused by large-scale density inhomogeneities in the pre-collapse core of the progenitor star [4] or convective instabilities in the neutrino-heated layer behind the SN shock [5, 6]. The kicks could also be a consequence of unequal momentum fluxes in a jet and an anti-jet that might be linked to the start of the SN explosion [7] or to the NS formation [2].

Alternatively or in addition, anisotropic neutrino (ν) emission from the nascent (“proto-”) neutron star (PNS) might transfer the momentum [8]. A “neutrino rocket engine” of the latter kind could result from the magnetic field-strength dependence of ν -matter interactions if extremely strong fields with hemispheric asymmetries build up in a PNS [9]. The ν transport also depends on the field direction, e.g., through parity violating corrections of weak interaction cross sections [10] or due to resonant flavor transitions [11]. In case of a significant dipole component such effects can lead to kicks of a few 100 km s^{-1} for magnetic fields in excess of 10^{15} G [2].

In this *Letter* we present new two-dimensional (2D) calculations of hydrodynamic instabilities during the onset of SN explosions which show that global asymmetries

and the PNS recoil can naturally grow to a sufficient size without invoking artificial initial conditions, extreme physical assumptions, or exotic ν physics. Our computations improve previous ones [6] with respect to numerical resolution, a full 180° lateral grid, and the treatment of ν transport, extending them also in the computed evolution time and model set.

Modeling concepts. We assume that the explosion is powered by ν -energy deposition between the PNS and the SN shock [12]. Although the currently most elaborate numerical models are not able to confirm the viability of this ν -heating mechanism, it is still the best-studied and most promising way to explode massive stars [13].

SN theory is currently hampered by our incomplete knowledge of the nuclear physics and ν interactions in the dense matter inside the PNS. This implies uncertainties for self-consistent models of the full problem, e.g. with respect to the magnitude of the ν fluxes emitted by the cooling PNS. Therefore, we replace the shrinking, high-density core of the PNS by a gravitating sphere whose radius coincides with the contracting, impenetrable inner boundary of our computational grid.

At this boundary, number and energy fluxes of ν and $\bar{\nu}$ of all three lepton flavors are imposed with chosen initial values and time dependence. In all simulations these boundary values were taken to be *isotropic* and were kept constant for a chosen period of time after shock formation (either 0.7 s or 1 s, within which 1/3 of the gravitational binding energy of the nascent NS was assumed to be radiated away in neutrinos). The grid boundary is located somewhat below the neutrinosphere of ν_e . It has an optical depth which, for typical ν energies, rises from few initially to several 100 at the end of the simulations. The use of this inner boundary allows us to explore the response of the collapsing SN core to different ν luminosities. Higher values of the latter lead to larger energy deposition behind the SN shock and therefore to more powerful explosions. The dominant heating reactions are

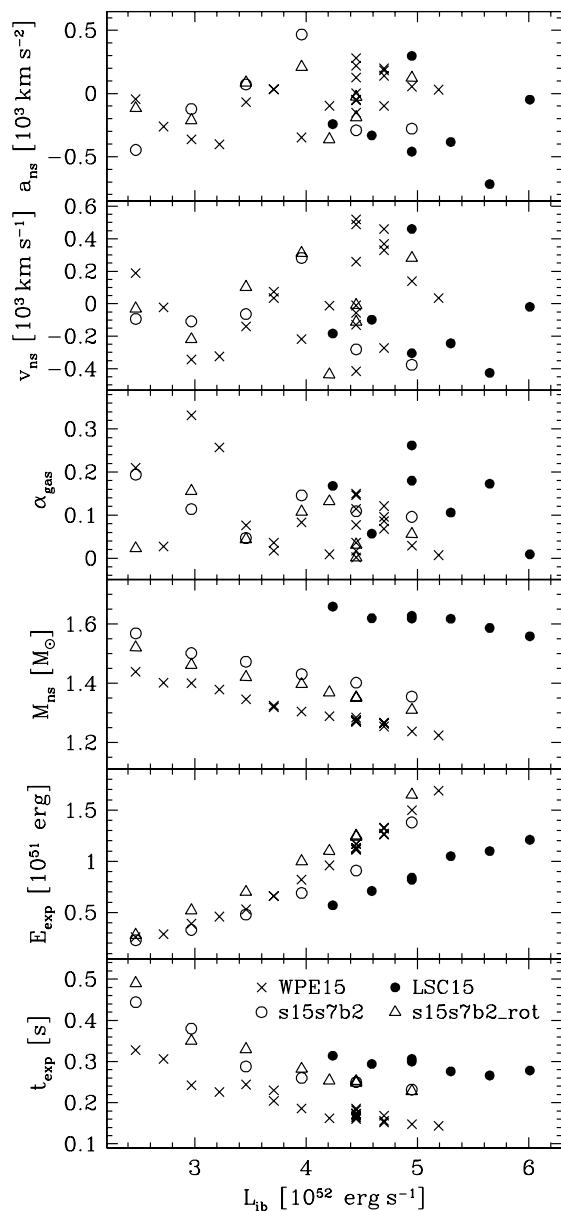


FIG. 1: Explosion timescale t_{exp} and, at one second after SN shock formation, explosion energy E_{exp} , NS baryonic mass M_{ns} , gas anisotropy parameter α_{gas} , NS recoil velocity v_{ns} , and NS acceleration a_{ns} (from bottom to top) vs ν_e plus $\bar{\nu}_e$ luminosity, L_{ib} , at the inner boundary. The symbols correspond to different models of $15 M_{\odot}$ stars, the triangles to a case including rotation (see text for details).

ν_e and $\bar{\nu}_e$ absorption on free nucleons.

The “lightbulb” approximation employed previously [6] ignored time retardation effects and did not take into account radial variations of the fluxes due to ν -matter interactions in the cooling and heating layers between PNS and SN shock. To improve on that in the present work, we make use of the zeroth moment of the Boltzmann transport equation in the form

$\partial_t L + \bar{c} \partial_r L = 4\pi r^2 \bar{c} Q_{\nu}^{-} - \kappa c L$. Here $L = L(r, t)$ is the total ν number flux or ν luminosity, respectively, Q_{ν}^{-} the rate of ν loss by the stellar medium per unit volume, $\kappa \equiv 4\pi r^2 \bar{c} Q_{\nu}^{+} / (Lc)$ the corresponding absorptivity, c the speed of light, and \bar{c} the “effective speed” of ν propagation, which is governed by diffusion at high densities and reaches c at large radii. The integration for L in radius r and time t (lateral flux components are ignored) can be done analytically when Q_{ν}^{-} , κ and \bar{c} are assumed to be constant within the cells of the numerical grid (consistent with this, the above equation was derived by employing $\partial_t \bar{c} = 0$). Instead of determining \bar{c} from the solution of the Boltzmann equation, we use an analytic representation in terms of the optical depth that was obtained from fitting results of detailed ν transport in the outer layers of the SN core. Neutrino-matter interactions via charged-current processes with nucleons, thermal pair creation, and scattering off nuclei, n , p , e^{-} , and e^{+} are evaluated by adopting Fermi-Dirac ν spectra with a temperature determined by the ratio between ν energy and number density. The chemical potentials of the spectra are taken to be equal to the equilibrium values at high optical depths and approach values near zero outside of the neutrinospheres.

This approximate ν transport retains the hyperbolic character of the transport problem, conserves lepton number and energy globally, and reproduces basic properties of accurate Boltzmann transport calculations despite of radical simplifications. It is coupled to our 2D hydrodynamics code by operator-splitting with a predictor-corrector step.

Our hydrodynamics code and equation of state are described in Ref. [14]. We typically use 400 geometrically spaced radial zones and one degree lateral resolution. The ν transport is solved in each angular bin separately. The 2D simulations were started some milliseconds after SN shock formation from detailed core-collapse models with fluid velocities randomly perturbed with an amplitude of typically 0.1%.

Results. Figure 1 shows four sequences of runs that followed the post-bounce evolution of different $15 M_{\odot}$ progenitors for one second. The crosses mark results based on the use of Model WPE15 [15], the solid dots of Model LSC15 [16], the open circles of Model s15s7b2 [17], and the triangles of a model with a structure like the latter but including rotation [13]. Starting with a rotation period of 12 s in the iron core [18], the post-collapse core spins differentially within 10–20 ms and speeds up as it contracts. The rotation period in the ν -heating layer varies between some 10 ms and several 100 ms [13].

Model LSC15, in particular, differs from the others by having significantly higher densities at the edge of the iron core and in the silicon shell (at a time when the cores have evolved to the same central density). This delays the start time, t_{exp} , of the explosion, reduces the explosion energy, E_{exp} , and leads to a larger NS baryonic

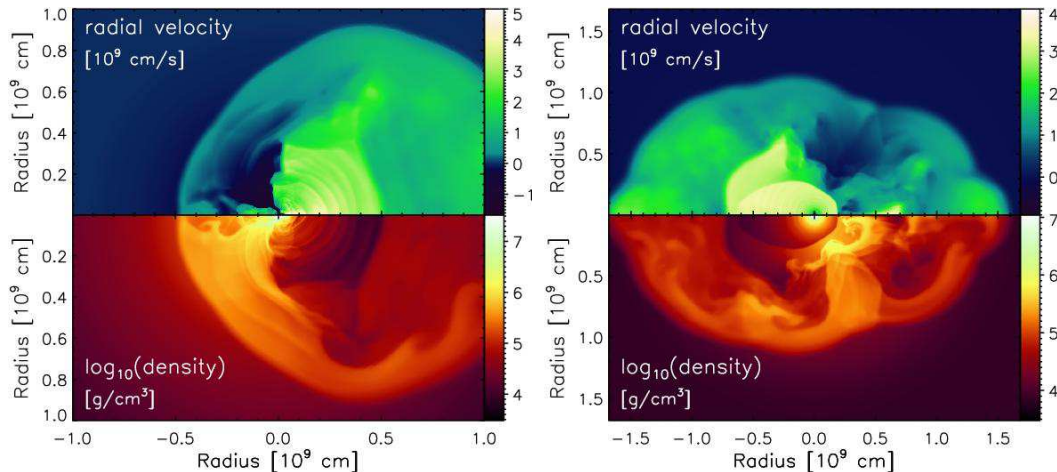


FIG. 2: Two models (based on progenitor WPE15) at 1 s after SN shock formation. The PNS is at the coordinate center. The left plot (scale reduced to show more details) displays a case with $L_{\text{ib}} = 2.97 \times 10^{52} \text{ erg s}^{-1}$, $E_{\text{exp}} = 0.4 \times 10^{51} \text{ erg}$, and a recoil velocity of $v_{\text{ns}} = -350 \text{ km s}^{-1}$. The model on the right has $L_{\text{ib}} = 4.45 \times 10^{52} \text{ erg s}^{-1}$, $E_{\text{exp}} = 1.2 \times 10^{51} \text{ erg}$, and $v_{\text{ns}} = +520 \text{ km s}^{-1}$.

mass, M_{ns} , for a given value of the boundary luminosity, L_{ib} , of ν_e plus $\bar{\nu}_e$ (Fig. 1). E_{exp} is defined as the total energy (internal plus kinetic plus gravitational) of the SN ejecta, integrated over all matter where the sum of the corresponding specific energies is positive, t_{exp} is the post-bounce time when E_{exp} reaches 10^{49} erg , and M_{ns} is the gas mass with densities above $10^{11} \text{ g cm}^{-3}$ plus the central point mass at one second.

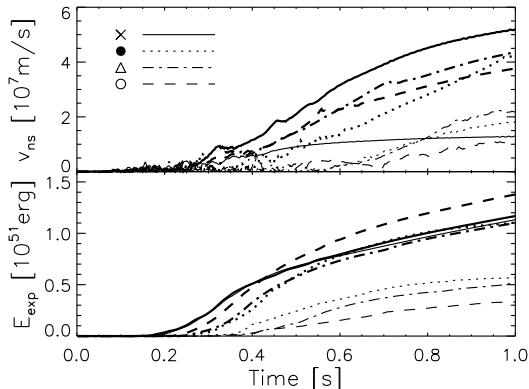


FIG. 3: Explosion energies (bottom) and NS velocities vs time for some simulations, showing large acceleration for cases with high v_{ns} (thick lines) even at 1 s after bounce. The symbols and line styles refer to the different model sequences of Fig. 1.

Figure 1 reveals the generic trend that a higher luminosity L_{ib} from the NS core causes the explosion to develop faster and to become more energetic. Because the period of mass accretion by the PNS is reduced, this implies a smaller NS mass. The time until the revived bounce-shock reaches a certain radius (correlated with t_{exp}) depends sensitively on the progenitor structure and the core ν luminosity. Rotation systematically increases the explosion energy by 20–50%, because centrifugal forces delay matter from being accreted onto the

PNS, and thus keep it in the ν -heating region to accumulate energy by ν_e and $\bar{\nu}_e$ absorption. This is basically in agreement with Ref. [13], where rotation was found to stabilize the standing accretion shock at a larger radius.

The layer between PNS and SN shock is convectively unstable according to the Ledoux-criterion because of a negative entropy gradient established by ν -energy deposition. Within $\sim 50 \text{ ms}$ after shock formation, convection sets in, supporting the start of the explosion [5, 6]. Initially the convective cells are small, but they begin to merge to larger entities. Three-dimensional (3D) simulations agree with this 2D result [19]. In case of rapid shock acceleration convection freezes, and small structures characterize the flow pattern until late times. However, when the stagnant shock expands slowly, small cells have time to merge to very large buoyant bubbles, separated by only a few narrow, supersonic downflows which carry low-entropy matter from the shock to the PNS surface. Moreover, global pulsations can develop with a dominance of low-order ($l = 1, 2$) modes. Consequently, the density distribution becomes highly aspherical and the explosion breaks out with a very large hemispheric or polar-to-equatorial asymmetry and corresponding shock deformation. In some cases a single long-lasting accretion funnel was found to persist for a second or even longer (Fig. 2). We emphasize that such structures did not preferentially occur along the polar (z -) direction of our spherical grid (where a coordinate singularity exists), but developed in arbitrary orientations.

The development of a stable, volume-filling $l = 1$ mode was proposed before [20]. It is supported by analytic arguments for thermal instabilities in fluid spheres [21] and is also observed in 3D hydrodynamic simulations of pulsating, convective red giant stars [22]. Determining the duration of such a phenomenon in the time-dependent environment of an exploding SN requires numerical modeling. The coherent, low-order oscillations of the fluid beneath the shock in our simulations look similar to the

recently discovered non-radial instabilities in adiabatic flow behind standing accretion shocks [23], which can be understood in terms of a “vortical-acoustic cycle” [24]. Doing numerical experiments we found that this phenomenon might indeed play a role, although Ledoux-instability due to ν -heating clearly starts the convective activity, and ν -cooling around the neutrinosphere seems to damp the energetic amplification of the feedback cycle between turbulence and pressure waves.

Anisotropic mass ejection can be associated with a high linear momentum taken up by the compact remnant. The corresponding asymmetry of the explosion is expressed by the parameter $\alpha_{\text{gas}} \equiv |P_{z,\text{gas}}|/P_{\text{gas}} \equiv |\int dm v_z|/\int dm |\vec{v}|$ where the integrals are performed over the ejecta mass and $P_{z,\text{gas}}$ is the gas momentum along the z -direction of the 2D grid. We find values for α_{gas} up to 0.33 (Fig. 1). The NS recoil velocities, $v_{\text{ns}} = \alpha_{\text{gas}} P_{\text{gas}}/M_{\text{ns}}$, can be close to zero but also more than 500 km s^{-1} . In some cases the acceleration, a_{ns} , continues on a high level beyond the 1 s of computed evolution (Figs. 1, 3) and significantly larger terminal velocities can be expected. It is mediated by the long-range gravitational force between the asymmetrically distributed ejecta and the PNS. Hydrodynamic forces play a role only as long as downflows reach the PNS, and anisotropic ν emission contributes insignificantly. There is no correlation of v_{ns} with the progenitor model. Rotation does not inhibit large kicks. The final recoil velocity depends stochastically on the initial seed perturbation and the highly nonlinear growth of the convective structures. There is also no obvious correlation with the explosion energy. Fig. 3 (by the thin and thick solid lines) and Fig. 1 (coinciding points) demonstrate that nearly the same E_{exp} can be associated with large or small v_{ns} .

Conclusions. We have shown that globally anisotropic mass ejection and NS acceleration can result from convective overturn and low-order oscillations of the ν -heated layer in a SN core. Low-mode convection turned out to develop from random seed perturbations in case of a slow onset of the explosion which gives the convective structures time to merge. This was disfavored by our previous choice of a strongly time-dependent, exponentially decaying core ν luminosity in Refs. [6, 14] but is possible with the less burst-like (because constant) L_{ib} assumed in this work. Our models suggest a consistent picture in which ν -energy deposition can be responsible for the SN explosion, for pulsar kicks, and for global asymmetries observed in many supernovae. The simulations need to be continued to later times to allow for quantitative conclusions on the morphological properties of the ejecta as, e.g., inferred from polarization measurements. Statistical information about the distribution of intrinsic pulsar velocities requires 3D simulations, a better fundamental understanding of the explosion mechanism, and a large sample of simulations for progenitor stars with different masses and rotation rates. The discussed kick mecha-

nism does not enforce a strict alignment of pulsar spin and space velocity, although the rotation axis of a star defines a naturally preferred direction, which might disfavor large misalignments.

We thank S.W. Bruenn and M. Rampp for post-bounce core-collapse models and M. Limongi and S. Woosley for their progenitor models. Support by the Sonderforschungsbereich 375 on “Astroparticle Physics” of the Deutsche Forschungsgemeinschaft is acknowledged. The simulations were done at the Rechenzentrum Garching and the Interdisciplinary Centre for Computational Modelling in Warsaw.

-
- [1] A.G. Lyne and D.R. Lorimer, *Nature (London)* **369**, 127 (1994); J.M. Cordes and D.F. Chernoff, *Astrophys. J.* **505**, 315 (1998); Z. Arzoumanian, D.F. Chernoff, and J.M. Cordes, *Astrophys. J.* **568**, 289 (2002); B.M.S. Hansen and E.S. Phinney, *Mon. Not. R. Astron. Soc.* **291**, 569 (1997); C. Fryer, A. Burrows, and W. Benz, *Astrophys. J.* **496**, 333 (1998)
 - [2] D. Lai, D.F. Chernoff, and J.M. Cordes, *Astrophys. J.* **549**, 1111 (2001)
 - [3] I.S. Shklovskii, *Sov. Astron.* **13**, 562 (1970)
 - [4] A. Burrows and J. Hayes, *Phys. Rev. Lett.* **76**, 352 (1996); D. Lai and P. Goldreich, *Astrophys. J.* **535**, 402 (2000)
 - [5] M. Herant, W. Benz, W.R. Hix, C.L. Fryer, and S.A. Colgate, *Astrophys. J.* **435**, 339 (1994); A. Burrows, J. Hayes, and B.A. Fryxell, *Astrophys. J.* **450**, 830 (1995)
 - [6] H.-T. Janka and E. Müller, *Astron. Astrophys.* **290**, 496 (1994); **306**, 167 (1996)
 - [7] R. Cen, *Astrophys. J.* **507**, L131 (1998); A.M. Khokhlov *et al.*, *Astrophys. J. Lett.* **524**, L107 (1999)
 - [8] N.N. Chugai, *Sov. Astron. Lett.* **10**, 87 (1984); A. Burrows and S.E. Woosley, *Astrophys. J.* **308**, 680 (1986)
 - [9] G.S. Bisnovaty-Kogan, *Astron. Astrophys. Trans.* **3**, 287 (1993); D. Lai and Y.-Z. Qian, *Astrophys. J.* **505**, 844 (1998)
 - [10] C.J. Horowitz and G. Li, *Phys. Rev. Lett.* **80**, 3694 (1998); P. Arras and D. Lai, *Astrophys. J.* **519**, 745 (1999); *Phys. Rev. D* **60**, 043001 (1999)
 - [11] A. Kusenko and G. Segrè, *Phys. Rev. Lett.* **77**, 4872 (1996); E. Nardi and J.I. Zuluaga, *Astrophys. J.* **549**, 1076 (2001)
 - [12] H.A. Bethe and J.R. Wilson, *Astrophys. J.* **295**, 14 (1985)
 - [13] R. Buras, M. Rampp, H.-T. Janka, and K. Kifonidis, *Phys. Rev. Lett.* **90**, 241101 (2003)
 - [14] K. Kifonidis, T. Plewa, H.-T. Janka, and E. Müller, *Astron. Astrophys.* **408**, 621 (2003)
 - [15] S.E. Woosley, P.A. Pinto, and L. Ensmann, *Astrophys. J.* **324**, 466 (1988); S.W. Bruenn, in *Nuclear Physics in the Universe*, edited by M.W. Guidry and M.R. Strayer (IOP, Bristol, 1993), p. 31
 - [16] M. Limongi, O. Straniero, and A. Chieffi, *Astrophys. J. Suppl.* **129**, 625 (2000)
 - [17] S.E. Woosley and T.A. Weaver, *Astrophys. J. Suppl.* **101**, 181 (1995)
 - [18] A. Heger, S.E. Woosley, N. Langer, and H.C. Spruit,

astro-ph/0301374

- [19] C.L. Fryer and M.S. Warren, *Astrophys. J. Lett.* **574**, L65 (2002)
- [20] M. Herant, *Phys. Rep.* **256**, 117 (1995); C. Thompson, *Astrophys. J.* **534**, 915 (2000)
- [21] S. Chandrasekhar, *Hydrodynamic and Hydromagnetic Instabilities* (Dover, New York, 1981), p. 234
- [22] P.R. Woodward, D.H. Porter, and M. Jacobs, in *3D Stellar Evolution*, ASP Conf. Series, Vol. **293** (ASP, San Francisco, 2003), p. 45
- [23] J.M. Blondin, A. Mezzacappa, and C. DeMarino, *Astrophys. J.* **584**, 971 (2003)
- [24] T. Foglizzo, *Astron. Astrophys.* **392**, 353 (2002)